



1 **Environmental lapse rate for high resolution land**
2 **surface downscaling: An application to ERA5**

3 **Emanuel Dutra¹, Joaquín Muñoz-Sabater², Souhail Boussetta², Takuya**
4 **Komori³, Shoji Hirahara³, and Gianpaolo Balsamo²**

5 ¹Instituto Dom Luiz (IDL), Faculdade de Ciências, Universidade de Lisboa, Portugal

6 ²European Centre for Medium-Range Weather Forecasts, United Kingdom

7 ³Global Environment and Marine Department, Japan Meteorological Agency

8 **Key Points:**

- 9 • Environmental lapse rate derived from atmospheric reanalysis vertical profiles agrees
10 with observational estimates
11 • Surface downscaling outperforms ERA5 but the impact of different ELR correc-
12 tions to the driving data is reduced
13 • Systematic biases in ERA5 near-surface temperature require further efforts from
14 modeling and data assimilation

Corresponding author: Emanuel Dutra, endutra@fc.ul.pt

-1-

This article has been accepted for publication and undergone full peer review but has not been through the copyediting, typesetting, pagination and proofreading process, which may lead to differences between this version and the Version of Record. Please cite this article as doi: 10.1029/2020GL046661

Abstract

In this study we derive the Environmental Lapse Rate (ELR) from vertical profiles of temperature in the lower troposphere, applying it to downscale air temperature of the new European Centre For Medium-Range Weather Forecasts (ECMWF) reanalysis ERA5, which replaces ERA-Interim (ERA-Interim). We focus over the Western US region, a data rich area with observations of daily maximum and minimum temperature (Global Historical Climatology Network, GHCN) and snow depth and soil temperature (SNOTEL). Observations indicate an ELR of -4.5 K km^{-1} in the region, lower than the commonly used -6.5 K km^{-1} . ERA5 ELR agrees with the observational estimates, with some overestimation in winter and limitations in the diurnal variability. The elevation correction of ERA5 temperature using different ELR showed the benefits of deriving ELR fields from ERA5 vertical profiles, when compared with a constant ELR. Simulations with the ECMWF land surface model, at 9 km resolution, driven by ERA5 using different ELR corrections showed the added value of the methodology, but the impact of different ELR corrections is limited. However, the validity of the downscaling method in reducing temperature to station altitude suggests there is sufficient generality for application at kilometer and sub-kilometer resolutions. By comparing the estimated representativity errors of observations with reanalysis, the improvements from ERA-Interim to ERA5 are mainly visible in the random component of the error. Large systematic biases remain, which require further attention from the modeling and data assimilation efforts, and limit the potential benefits of ELR corrections.

1 Introduction

High spatial and temporal resolution near-surface climate and weather conditions are paramount for the understanding, monitoring and forecasting of ecological, hydrological, and climate change processes, among others (e.g. Behnke et al., 2016; Maraun et al., 2010; Maselli et al., 2012; Tobin et al., 2012). Near-surface air temperature and precipitation are key fields due to their relevance in the evolution of surface and subsurface conditions (e.g. vegetation, groundwater), which are then used to drive process based or statistical models. High spatial resolution is also becoming increasingly important in climate change studies with examples such as the Coordinated Regional Climate Downscaling Experiment (CORDEX) (e.g. Endris et al., 2013; Soares et al., 2017). A common approach to enhance the spatial resolution is statistical or dynamical downscaling. Statistical downscaling can be very effective, in particular if using local observations, (e.g. Winstral et al., 2017; Maraun et al., 2010; Cao et al., 2017). Dynamical downscaling of global atmospheric reanalysis, weather forecasts or climate change projections is a widely used methodology to enhance the spatial information (Soares et al., 2012). Dynamical downscaling with limited area (or regional) atmospheric models has a significant computational cost, but provides a physically consistent description of the land and atmosphere (e.g. relation between temperature, humidity, radiation, clouds, precipitation, etc), while suffering from model limitations (e.g. biases). Statistical downscaling is based on statistical relationships to predict the evolution of local variables from large-scale variables. It is computationally cheaper, but requires observations, which are not always available, and the spatial consistency between downscaled fields can be difficult to achieve.

Temperature near the surface varies with altitude accordingly to the environmental lapse-rate (ELR). The ELR depends on the overlying air masses, large-scale situation and local effects (Sheridan et al., 2010). The characterization of the ELR has several applications, in particular to downscale global/regional numerical weather predictions, reanalysis and climate projections in complex terrain regions. From an observational point of view, complex terrain regions also constitute a challenging environment due to the difficulties associated with the installation and maintenance of observational networks. The use of a linear lapse rate for altitude correction of temperature is a common practice (e.g. Dodson & Marks, 1997). The main challenge is the definition of the

67 ELR. Optimally, provided that there is a high density and homogeneous distribution of
68 stations, this information could be used. However, such station density is not available
69 globally. Accounting for elevation differences is fundamental for temperature interpo-
70 lations over complex terrain regions (Stahl et al., 2006). There are numerous observa-
71 tional indications that ELR varies in time and space and that the commonly used con-
72 stant value of -6.5 K km^{-1} is too high (e.g. Jobst et al., 2017; Shen et al., 2016; Wang
73 et al., 2018; Minder et al., 2010). Without local observations spanning a wide range of
74 altitude bands, atmospheric vertical profiles have also been used to estimate the ELR.
75 Gao et al. (2012) evaluated several ELR in the Alps using station information. They found
76 that compared with a constant climatology (Liston & Elder, 2006) the ELR derived from
77 the pressure levels of ERA-Interim atmospheric reanalysis (ERA-Interim, Dee et al., 2011) had
78 a good performance. This methodology was also found to perform well when tested in
79 the Tibetan Plateau (Gao et al., 2017; Gerlitz et al., 2014).

80 The use of ELR for elevation corrections between model and station temperature
81 is widely accepted, but other surface characteristics such as snow depth or soil temper-
82 ature are also expected to depend significantly with altitude. Model simulations with
83 a land surface model (hereafter surface simulations) forced with downscaled near-surface
84 meteorology can be a compromise to enhance the spatial resolution but with a consid-
85 erable lower computational cost when compared with a dynamical downscaling using a
86 regional or limited area atmospheric model. Bernier et al. (2011) carried out surface sim-
87 ulations at 100 meters resolution in a complex Alpine region in Vancouver Canada show-
88 ing the added value of this methodology in simulating snow evolution. This was further
89 investigated by Ioannidou et al. (2014) to evaluate surface winds downscaling.

90 In this study we aim to evaluate the effect and impact of different ELR corrections
91 to downscale the new European Center for Medium-Range Weather Forecasts atmospheric
92 reanalysis ERA5 (Hersbach et al., 2018). We focus over the Western US region due to
93 the amount of available observations in the Global Historical Climatology Network - Daily
94 (GHCN), Version 3 (Menne, Durre, Korzeniewski, et al., 2012) and the Natural Resources
95 Conservation Service (NRCS) SNOTEL network, as well as its complex terrain char-
96 acteristics. As a first step, estimates of the ELR were derived from observations of daily
97 maximum, minimum and mean temperature and then ERA5 temperature was reduced
98 to the stations altitude using different ELR corrections. The ELR corrections include
99 a constant ELR commonly used of -6.5 K km^{-1} and spatially and temporally varying
100 ELR fields derived from ERA5 lower troposphere thermodynamic vertical profiles. Sur-
101 face simulations (or offline) with the ECMWF land surface model HTESSEL were car-
102 ried out at 9km driven by ERA5 hourly surface downward fluxes (rainfall, snowfall, long-
103 wave and shortwave radiation) and near-surface state (temperature, specific humidity,
104 wind speed and pressure). ERA5 fluxes and near-surface state were interpolated to the
105 9km resolution, whereas temperature (also humidity and pressure) were corrected for el-
106 evation differences between ERA5 (31 km) topography and the 9km resolution using dif-
107 ferent ELR corrections. The simulations of snow depth and soil temperature were eval-
108 uated and compared with both ERA5 and ERA-Interim. The 9 km resolution was chosen for
109 practical reasons as the highest global resolution currently operationally run at ECMWF,
110 however this does not represent a limitation of the applicability of the downscaling method.
111 Finally, an estimate of observational uncertainty was performed to assess the role of spa-
112 tial sampling and altitude variability and compared with ERA5 and ERA-Interim reanalysis.
113 The following section presents the detailed datasets and methodologies, followed by the
114 results with the key conclusions in the last section.

2 Methods

2.1 Data

2.1.1 Observations

The observations of daily maximum temperature (dtmax) and daily minimum temperature (dtmin) were taken from GHCN. GHCN includes daily land surface observations from around the world, from different networks. If observed, the station dataset includes dtmax, dtmin, total precipitation, snowfall, and snow depth (Menne, Durre, Vose, et al., 2012). The GHCN data were processed from the original format for the period 1 June 2009 to 31 May 2014 restricting the data to a region between 125° to 100° West and 30° to 50° North (western United States - WUS). This region was selected due to the high density of stations and elevation variability. A missing data screening was applied to retain only stations with at least 80% of available data for the period considered. After the regional and temporal filters 2941 stations were retained (Figure 1a) with dtmin and dtmax data with at least 80% of available data for the 5 years considered. The daily mean temperature (dtmean) was also considered in the analysis. Since dtmean is not available in GHCN, it was computed as the arithmetic mean between Tmin and Tmax. This simple approach can lead to some deviations from the actual daily mean temperature (Weiss & Hays, 2005; Dall’Amico & Hornsteiner, 2006). However, since GHCN only contains dtmin and dtmax the simplest option for the daily mean computation was selected.

In addition to the GHCN air temperature observations, the Natural Resources Conservation Service (NRCS) SNOTEL network observations of snow depth and soil temperature at 5 cm depth were used in the model evaluation. The observations were processed for the same time period and region as GHCN, retaining only stations with 80% of available daily data. This resulted in 313 stations with snow depth (Figure 1b) and 260 stations with soil temperature (Figure 1c). The soil temperature data from this network has been used to evaluate ECMWF soil temperature performance (Albergel et al., 2015). The GHCN dataset also includes snow depth, but only the NRCS-SNOTEL network was used in this study. This network has been designed to collect snow and climate data in western US mountainous regions, which is the environment expected to be mostly affected by model topography and resolution.

2.1.2 Reanalysis

In this study we focus on the the most recent ECMWF atmospheric reanalysis ERA5 (Hersbach et al., 2018). This is the latest and fifth generation of atmospheric reanalysis produced by ECMWF under the Copernicus Climate Change Service (C3S). This new reanalysis replaces the widely used ERA-Interim reanalysis (Dee et al., 2011) from 1979 to close to real time as well as an extension back to 1950. Compared with ERAI, ERA5 has several enhancements, including: (i) higher spatial horizontal resolution (about 75 km in ERAI to 31 km in ERA5), (ii) higher vertical resolution (from 60 levels in ERAI to 137 in ERA5), (iii) higher temporal resolution of archived data (3-hourly in ERAI to hourly in ERA5) and (iv) a recent model and data assimilation systems. Regarding the model and assimilation changes, there are numerous improvements benefiting from more than 10 year of development of the numerical weather prediction system at ECMWF. For example the land surface scheme has suffered a major upgrade, that lead to a land-only interim reanalysis ERA-Interim/land (Balsamo et al., 2015), including a revised soil hydrology (Balsamo et al., 2009) and snow scheme (Dutra et al., 2010). Other examples of model changes include revisions in the convection and diffusion (Bechtold et al., 2008). ERA5 dtmin and dtmax were calculated from the 2-meters temperature hourly analysis, and dtmean computed as the arithmetic mean of dtmin and dtmax to be consistent with the processing of GHCN.

165 2.2 ELR estimates

166 The ELR is defined as the rate of temperature change with height and can be com-
167 puted as:

$$168 \Gamma = \frac{DT}{DZ} \quad (1)$$

169 where Γ is the ELR (K km^{-1}), DT is the temperature difference (K) between two lay-
170 ers DZ , assuming 0 at the land surface. Γ is normally negative with a lower limit of -10
171 K km^{-1} for the dry-adiabatic lapse rate, taking higher values with increased moisture.
172 In particular situations, the ELR can take positive values, i.e. temperature increases with
173 height leading to temperature inversions. These situations occur mainly in stable condi-
174 tions or due to large-scale subsidence.

175 2.2.1 Observations

176 The ELR was estimated from the in-situ GHCN observations via linear regression
177 of the observed temperature versus the station altitude in the form:

$$178 T_i = \Gamma_O \times Z_i + T_0 \quad (2)$$

179 where T_i (K) is the station observed mean temperature (taken over a specific period) with
180 the associated altitude Z_i (Km), and the estimated Γ_O is computed by the regression
181 as well as T_0 (the estimated temperature at altitude 0). The temperature averaging pe-
182 riod considered included the full 5 years and the mean monthly climatology. Day by day
183 and month by month calculations were performed but the regression quality was poor
184 in many areas, which can be associated with synoptic variability affecting each station
185 differently. The linear regression requires the definition of a group of stations. The method-
186 ology chosen was to split the study area in a regular grid of 1° by 1° and to perform the
187 regression for all stations falling within each area with a 2° search radius. This leads to
188 some overlap, i.e. one station can be used in several area calculations. Only points with
189 at least 30 stations and with a standard deviation of the stations altitude higher than
190 400 m were considered. These two constraints were imposed to guarantee a robust lin-
191 ear regression. Furthermore, only regressions with a coefficient of determination (R^2) above
192 0.5 were considered to mask out problematic areas (e.g. snow vs snow-free, highly in-
193 homogeneous areas, coastal areas). This approach transforms the spatial distribution of
194 surface temperature for different stations in each 1° by 1° area into an estimate of ELR.
195 This approach has two main limitations (i) it relies on the elevation variability among the
196 stations and (ii) assumes that temperature at stations in different elevations are repre-
197 sentative of the mean lower troposphere vertical structure. Sounding data could be used
198 also to derive the ELR, but since most of the freely available sounding data has been used
199 by the data assimilation in ERA5, this would likely result in similar estimates as those
200 done using ERA5 vertical profiles.

201 2.2.2 Reanalysis

202 The ELR was estimated from the temperature vertical profiles of ERA5 in the lower
203 troposphere. A similar methodology to derive the ELR was proposed by Gao et al. (2012,
204 2017) over the French Alps and Tibetan Plateau for temperature elevation corrections.
205 Gao et al. (2017) estimated the ELR from the temperature differences between differ-
206 ent pressure levels. We propose a modification using the original model levels that fol-
207 low the model topography. We compute the ELR as in equation 1 between 16 combi-
208 nations of model levels centered between: model level 124 (500 m above the surface) and
209 model level 116 (1200 meters above the surface). These 16 estimates of the ELR are then
210 averaged, considering only negative values, i.e. excluding temperature inversions. Sev-
211 eral combinations of upper and lower limits were tested and the levels between 500m to
212 1200m were chosen to avoid sharp inversions near the surface as well as subsidence in-
213 versions. Even with the limits at 500m and 1200m inversions are captured, and an ELR

214 of zero is assumed in those situations. On a global scale the main regions with positive
215 (set to zero) ELR are associated with large-scale subsidence either linked with the Hadley
216 circulation (over the oceans) or winter anticyclonic subsidence and very stable conditions
217 in northern latitudes land masses.

218 The ELR was estimated using the vertical profiles of temperature and specific hu-
219 midity (the latter required to compute the altitude from the model levels), using two time
220 periods averaging: (i) daily means of the analysis at 0/6/12/18 UTC resulting in daily
221 global fields of ELR (daily ELR); (ii) the 5 years mean monthly analysis resulting in one
222 global field for each calendar month (mean climatological ELR). In addition to these
223 two methods (see Table 1), a globally and temporally constant ELR of -6.5 K km^{-1} (clr)
224 and -4.5 K km^{-1} (clrO) were also included. The constant value of -6.5 K km^{-1} is widely
225 used in many applications (e.g. Maurer et al., 2002; Cosgrove et al., 2003) derived from
226 estimates of the mean free atmosphere lapse rate. The constant ELR of -4.5 K km^{-1} was
227 taken from the observations estimates (see section 3.1).

228 2.3 Land Surface simulations

229 The ERA5 lowest model level (about 10m height) fields of air temperature, spe-
230 cific humidity, wind-speed and surface pressure along with the downwelling fluxes of short-
231 wave and longwave radiation and solid and liquid precipitation were used to perform sur-
232 face (or offline) simulations. We use the same land surface model version as used in ERA5
233 which is very similar to the version used for ERA-Interim/Land (Balsamo et al., 2015).
234 The ERA5 meteorological fields are taken from the +1h to +12h forecasts initialized at
235 06UTC and 18UTC, resulting in continuous hourly time series.

236 The surface simulations were performed at a higher resolution than ERA5, match-
237 ing that of ECMWF high resolution weather forecasts of about 9km. The simulations
238 were initialized in January 2009 extending until May 2014. The first 5 months of sim-
239 ulation were considered as as spin-up. Since the evaluation focuses only on near-surface
240 variables, possible effects of spin-up (e.g. adjustment of deep soil moisture/temperature)
241 have a small impact. Four simulations were performed differing on the meteorological
242 forcing and are listed in Table 1. The default configuration is bilinear interpolation of
243 the forcing fields (HTbil) while the remaining three were adjusted to the differences be-
244 tween ERA5 (31km) and the high resolution (9 km) model orography using different ELR
245 estimates. The correction is the following: (i) relative humidity is computed from the
246 uncorrected forcing; (ii) air temperature is corrected using the ELR and altitude differ-
247 ence; (iii) surface pressure is corrected assuming the altitude difference and updated tem-
248 perature; and (iv) specific humidity is computed using the new surface pressure and tem-
249 perature assuming no changes in relative humidity.

250 One additional simulation was carried out for the same period using ERAI forc-
251 ing and resolution (about 75 km), (hereafter HTei).HTei has the same configuration as
252 ERA-Interim/Land but used the same model version as ERA5, and there was no pre-
253 cipitation correction as in ERA-Interim/land. Despite the similarities, this new simu-
254 lation was performed to guarantee that all surface simulations presented in this study
255 were carried out with the same model version and consistent with ERA5.

256 2.4 Evaluation metrics

257 In the simulations evaluation four main scores are used: (i) the mean bias (simulation-
258 observation, BIAS), (ii) the mean absolute error (MAE), (iii) the standard deviation of
259 the error (standard deviation of the differences between the simulation and observation
260 - STDE) and (iv) the temporal correlation (PCORR). While the BIAS and MAE indi-
261 cate systematic errors, the STDE (also known as the unbiased root mean square error)
262 can be interpreted as the random component of the error. The scores are computed for

263 each station and considered time period. The metrics are presented as the median of the
264 scores of all stations to avoid outliers which could affect the mean of the score. Confi-
265 dence intervals of the median scores were estimated with a 1000 samples bootstrapping
266 with replacement to account for stations sampling uncertainty.

267 2.5 Observations representativity

268 The representativity of the in-situ temperature observations was estimated by com-
269 puting the MAE and STDE of each station against the mean over a certain radius. The
270 calculation was performed in the following steps:

- 271 1. For each individual station a group of stations was created with a distance smaller
272 than a particular radius (area);
- 273 2. The spatial mean of all stations in that radius was computed to represent area mean;
274 This included two calculations: (i) including all stations and (ii) including only
275 stations with a similar altitude, defined as altitude within +/- 100m from the mean
276 in the area;
- 277 3. The MAE and STDE was computed for each station against the area mean com-
278 puted in (2); Steps 1-3 were repeated for all stations and search radius from 30
279 to 150 km;

280 Only areas (in point 1) with at least 10 stations were retained and the number of areas
281 and mean number of stations in each region was saved. Since the areas are defined start-
282 ing from each station, there is a significant overlap, i.e. the same stations are accounted
283 in several regions. This procedure can be seen as a smoothing filter to generate the area
284 means that are then used to compute the MAE and STDE as measures of the spatial
285 representativity of the observations. The restrictive selection criteria of similar altitude
286 stations was introduced to estimate how much of the representativity errors can be as-
287 sociated with altitude differences.

288 3 Results

289 3.1 ELR from observations and reanalysis

290 The high density temperature observation and terrain variability in the WUS re-
291 gion allows the estimation of the ELR based on in-situ stations. Figure S1 in the sup-
292 porting information shows the stations spatial distribution as well as the aggregated num-
293 ber of stations, mean elevation and standard deviation of the stations elevation in each
294 of the regular areas considered. The restriction of at least 30 stations with elevation vari-
295 ability, measured by the standard deviation, excluded mostly the eastern region of WUS
296 domain due to the reduced elevation variability.

297 The observational estimates of the ELR show a clear annual cycle (Figure 2d). Daily
298 ELR estimates were calculated but the results were very noisy, which could be related
299 to the different times of occurrence of the temperature extremes in each stations. The
300 temporal averages considered in the study (e.g all days in each calendar month - Fig-
301 ure 2d) filter out the random timing differences resulting in consistent temporal (mean
302 climatology) and spatial fields, comparable with the independent estimates from ERA5.
303 The estimates depend on the variable taken: lower absolute ELR when using the daily
304 minimum temperature and higher absolute ELR when using the daily maximum tem-
305 perature. These results are expected since nocturnal low-level conditions tend to be more
306 stable, resulting in less intense ELR when using the daily minimum temperature. The
307 comparison between observations and ERA5 ELR shows a reasonable agreement when
308 considering the spatial averages over the domain (Figure 2d). The South-North gradi-
309 ent is also captured (annual fields in Figure 2e,f and Figure S2 for the winter and sum-
310 mer months). The mean absolute difference of the ERA5 ELR compared with the sta-

tion estimates is 1.5 (2), 1.2 (3.1) and 1.8 (1.5) K km⁻¹ for the annual, winter and summer periods, respectively (between brackets are the mean absolute differences of a constant ELR of -6.5 compared with the station estimates). The linear regression slopes in Figure 2a,b,c are always below 1 suggesting a reduced sensitivity of ERA5 ELR compared with the observational estimates. During summer ERA5 ELR estimates have a small sensitivity for large absolute ELR with a general overestimation (Figure 2b), which is also present in the annual ELR (Figure 2a), but less pronounced. This is particularly evident in the Northern area of the domain. Further analyses did not identified any particular characteristic that could explain these differences. It is likely that some of the differences arise from the uncertainties introduced by different assumptions used to derive the ELR from ERA5 vertical profiles and from the spatial and vertical variability of the stations observations.

3.2 Elevation correction of ERA5 temperature

Meteorological stations are usually located in easily accessible areas, resulting in a sampling bias of lower altitudes when considering the local topography. This is illustrated when comparing the altitude differences, defined as the differences between ERA5 orography and the station elevation (see Figure 1a and Figure S3b), with a higher frequency of stations below ERA5 orography than above. In this section we compare ERA5 dtmin, dtmean and dtmax with ERA5 temperatures reduced to the station elevation using different ELR corrections: constant lapse rate of -6.5 and -4.5 K km⁻¹ (clr, clrO), monthly climatology fields of ELR derived from ERA5 (mlr) and daily ELR fields derived from ERA5 (dlr). The temperature differences, defined as the difference between model and observations, when organized as function of the elevation differences highlight the role of elevation in the mean bias (Figure 3). The slope of the linear regression between these temperature differences as function of elevation differences can be also interpreted as an estimate of the ELR required to correct model data, and the correlation coefficient a measure of the linear dependence. The dependence of ERA5 mean temperature bias on elevation differences is clear for dtmax and dtmean while for dtmin the relation is not so strong (Figure 3 and Table 2, note the higher correlations for dtmax and dtmean when compared with dtmin). This is further illustrated when considering only summer or winter months (Table 2). These results indicate that the bias relation with altitude is not constant (or the ELR required to correct model data). Taking dtmean for the full period the optimal ELR correction for the region is -4.5 K km⁻¹. Considering the different ELR corrections, none consistently outperforms the others. The dlr and mlr provide the best corrections for dtmean consistently for the full period or when considering only winter or summer months. In general, all corrections fail to capture the high ELR for dtmax and low ELR for dtmin.

The added value of the ELR correction to ERA5 is clear for dtmax (see Figure 4) in terms of a reduction of the mean absolute error and bias. For the standard deviation of the error, there is no change in case of a constant ELR, but the time varying ELR (dlr or mlr), increases the error. There is no clear added value of a variable ELR correction when compared with an optimal constant ELR (clrO - derived for this area as -4.5 K km⁻¹) when considering all stations and these metrics. Independently from the ELR chosen, the corrections for dtmax and dtmean are always positive and more pronounced during summer when compared with winter. For dtmin the ELR corrections are neutral or detrimental, which is consistent with the previous analysis of the temperature bias relationship with elevation differences (Figure 3). If we consider only stations above or below ERA5 orography (see Figure 5 for the bias, and Figures S4 and S5 for the remaining scores) the results highlight a large discrepancy in the correction impact. For stations above model orography (Figure 5a-c) all ELR corrections reduce the temperature biases during summer while deteriorate during winter, with clr being the worst. While during summer ERA5 has a warm bias in these stations, which is expected, there was a neutral to negative bias during winter. The ELR correction leads to a cold bias which is then reflected in the MAE

364 deterioration. Considering only the stations below ERA5 orography (valley stations, Fig-
365 ure 5d-f) the ELR corrections are effective for dtmax and dtmean with average reduc-
366 tions of 40% of the MAE. For dtmin, the improvements are smaller with even some de-
367 terioration during summer. In these valley stations, ERA5 shows a strong cold bias (al-
368 most -5 K) for dtmax and a much smaller cold bias for dtmin (about -1.3 K), suggest-
369 ing an underestimation of the amplitude of the diurnal cycle, which is independent from
370 the relative elevation difference from ERA5, and likely related with local effects.

371 **3.3 Land Surface Downscaling**

372 The previous sections focused on the near surface temperature and different ap-
373 proaches to account for stations altitude differences in respect to the model orography.
374 Other land-surface variables, such as snow depth and soil temperatures are also expected
375 to vary strongly with altitude as response to air temperature changes. In this section we
376 focus on the SNOTEL snow depth and 5 cm deep soil temperature observations (see Fig-
377 ure 1b-c). ERA5 biases in respect to the elevation differences (see Figure S6) shows that
378 soil temperature biases are tightly correlated with altitude differences during summer
379 while during winter this relation is not so evident. In winter, the presence of snow and
380 its thermal insulation effects (Dutra et al., 2011) is likely to dominate over the altitude
381 differences. For snow depth we see a positive relationship with elevation differences re-
382 sulting from both temperature effects (colder in altitude) and enhanced precipitation/snowfall
383 with altitude. Considering the tight relationships found between ERA5 biases and ob-
384 servations as functions of altitude differences, in the following results we investigate the
385 potential added value of higher resolution land-surface only simulation with different ap-
386 proaches to account for the ELR in the temperature forcing correction (see Table 1). The
387 results are benchmarked against those of ERAI, including also ERA5 to evaluate the im-
388 pact of the surface downscaling when compared with the ERAI to ERA5 evolution. Fur-
389 thermore, an additional surface simulation driven by, and at the same resolution as, ERAI
390 (HTei) but using the same surface model as ERA5 is evaluated to provide the impact
391 of the surface model changes.

392 The soil temperature evaluation (Figure 6), shows a general improvement from ERAI
393 to ERA5 in all metrics. The added value of the surface downscaling is mainly visible dur-
394 ing winter in terms of variability (reduction of 60% of the STDE in respect to ERAI, and
395 higher correlations). During winter HTei also shows some improvements in respect to
396 ERAI (35% reduction of STDE), and similar to ERA5 (45% reduction of the STDE),
397 highlighting the benefits of the model changes from ERAI to ERA5. During summer the
398 impact on soil temperature of the surface downscaling is smaller than in winter, but there
399 are still some improvements in terms of the MAE and correlation with some deteriora-
400 tion of the STDE. Finally, there is no clear difference between the three tested methods
401 of the ELR temperature correction in terms of soil temperature skill.

402 The snow depth evaluation (Figure 7) shows a clear evolution from ERAI to HTei
403 with a reduction of the bias, MAE, STDE and increased correlation. ERA5 further im-
404 proved HTei, which is likely associated with a better meteorology quality (Albergel et
405 al., 2018; Beck et al., 2019). The benefits of the surface downscaling are mainly visible
406 in spring suggesting the added value of the temperature corrections during the ablation
407 season. Taking the spring normalized MAE in respect to ERAI we see an error reduc-
408 tion of: 15% in HTei, 42% in ERA5 and 52% in HTclr/HTmlr/HTdlr. As for the soil
409 temperatures, there is no clear difference between the different methods of ELR temper-
410 ature corrections.

411 **3.4 Stations representativity**

412 Comparing model simulations with in-situ observations raises several questions re-
413 garding spatial representativity. Models normally represents a certain quantity as the

414 mean over a grid-box while in-situ observations are local, and depending on the weather
415 conditions and location, their spatial representativity can vary significantly. This raises
416 a question: what is the representativity uncertainty of the in-situ data and how does this
417 varies with the spatial scale considered? Considering the reasonably high density net-
418 work over the considered Western U.S region, an estimate of the spatial uncertainty de-
419 rived from observations was carried out as described in the methods section. The results
420 applied to the GHCN dtmin, dtmean and dtmax (see Figure 8) provide an estimate of
421 the in-situ representativity uncertainty. This can be also interpreted as the minimum MAE
422 and STDE that should be expected from comparing grid-averaged versus individual sta-
423 tions. This could be further interpreted as the minimum expected errors (or benchmark)
424 when comparing model data with the in-situ observations, i.e. we should not expect a
425 MAE or STDE of zero but a minimum value linked with the stations sampling and char-
426 acteristics. The results (in Figure 8) show that both MAE and STDE increase with in-
427 creased radius (i.e. larger areas) and are larger for dtmax than for dtmin, and dtmean
428 has the lower values. The dtmax and dtmin MAE becomes similar when considering only
429 stations with similar altitudes (comparing Figure 8b solid vs dashed red and blue lines).
430 This indicates a higher sensitivity the daily maximum temperature to elevation differ-
431 ence than daily minimum temperature. The large STDE of dtmax, when compared with
432 dtmin, is partially associated with a larger temporal variability (day-to-day) of dtmax.
433 The altitude differences explain almost 50% of the MAE while for the STDE the alti-
434 tude differences impact is smaller. These results are expected as systematic differences
435 driven by altitude are significant while random differences are associated with local ef-
436 fects where altitude alone does not explain the differences.

437 By comparing ERAI and ERA5 errors with the observational MAE and STDE es-
438 timates it is possible to assess on one hand the evolution of the reanalysis and on the
439 the other hand how far the reanalysis are from the expected minimum. For this com-
440 parison, only stations with altitude differences lower than 100 m to both ERAI and ERA5
441 orography were considered (588 stations). Since the reanalysis metrics are computed only
442 for stations with similar altitudes, the benchmark values (or lower limits) should be the
443 estimates using only stations with similar altitudes (dashed lines in Figure 8b,c). For the
444 MAE, there was a slight increase of the error from ERAI to ERA5 of dtmin and dtmax
445 with a slight reduction of dtmean. In the case of the STDE there was a clear reduction
446 from ERAI to ERA5, particularly for dtmax. The reduction of the STDE highlights the
447 model and data assimilation advances in reducing random errors from ERAI to ERA5,
448 likely associated with synoptic variability. However, the stagnation of the systematic er-
449 rors despite model and resolution enhancements suggests that further focus on model
450 processes (e.g. land-surface, boundary layer, clouds, radiation) are still required.

451 **4 Conclusions**

452 The use of the in-situ GHCN network to estimate the ELR shows a clear annual
453 cycle as well as diurnal variations, with lower ELR for dtmin when compared with dt-
454 max, and higher values during summer (JJA) when compared with winter (DJF). These
455 results are consistent with the findings of Minder et al. (2010) over the Cascade Moun-
456 tains. The estimated ELR from ERA5 vertical profiles is reasonably consistent with the
457 observational data, both temporally and spatially, when using dtmean, with a tendency
458 for overestimation. The proposed methodology to derive the ELR from ERA5 vertical
459 profiles only provides a daily mean estimate, which is a limitation considering the strik-
460 ing variability seen in the observations between daily maximum and minimum temper-
461 atures and ELR. Inversions are neglected, contributing to the overestimation of the de-
462 rived ELR and limiting its application in typical inversion conditions (e.g. clear sky cold
463 nights).

464 The elevation correction of ERA5 temperature to the GHCN stations elevation us-
465 ing different ELR corrections (from constant to daily varying fields) showed that there

466 is no single approach outperforming the others consistently. However, considering the
467 daily mean temperature, the temporally and spatially varying ELR derived from ERA5
468 vertical profiles (mlr and dlr) provides the best correction by removing most of the er-
469 ror dependence on altitude. However, when evaluating the temperature elevation cor-
470 rections to station altitude there is no significant added value of the variable ELR when
471 compared with the constant ELR. Additionally, the performance of the corrections for
472 dtmin and dtmax and for stations below or above the model orography varies significantly.
473 Our results highlight the drawbacks of the simple ELR correction (even when consid-
474 ering a spatially and temporally varying ELR) which fails to capture changes in the di-
475 urnal temperature range, as well as local effects. In all cases, the temporally and spa-
476 tially varying ELR (mlr and dlr) leads to an increase of the random error (standard de-
477 viation of the error), which is a considerable limitation of this approach. Therefore, the
478 use of this approach when correcting model data to a particular location is mainly suit-
479 able for the daily mean temperature, while caution must be taken for daily minimum
480 and maximum temperatures. The systematic biases in ERA5 are due to both local ef-
481 fects, which are not strictly dependent on altitude (Steinacker et al., 2007; Pepin, 2005;
482 Vosper & Brown, 2008), and physical processes representation in the model (e.g. radi-
483 ation, boundary layer, surface heterogeneities), leaving altitude differences as a second
484 order effect to explain the mixed impact of the ELR corrections tested.

485 The response of the land surface to the altitude changes was evaluated by down-
486 scaling ERA5 near-surface meteorology to drive the land-surface model, accounting for
487 different ELR corrections in temperature. The validation was focused on the SNOTEL
488 network of snow depth and 5 cm deep soil temperature, comparing the evolution from
489 ERAI to ERA5 and the surface high resolution (9km) simulations. For soil temperatures
490 there is a clear improvement from ERAI to ERA5 with the surface downscaling further
491 improving the standard deviation of the error and temporal correlations during winter.
492 For snow depth the added value of the surface simulations when compared with ERA5
493 is mainly restricted to the melting season. This surface only downscaling methodology
494 can also benefit from other corrections. An example would be precipitation, consider-
495 ing the recent advances in generating multi-product precipitation estimates (Beck et al.,
496 2019)). Other corrections such as downward solar radiation shading by topography (Varley
497 et al., 1996) or rainfall/snowfall partitioning (Tobin et al., 2012) could be also explored.

498 By comparing the estimated representativity errors of the in-situ GHCN temper-
499 ature observations with the ERAI, ERA5 and downscaled errors, the improvements from
500 ERAI to ERA5 were reasonably limited (considering the expected improvements by res-
501 olution alone), and mainly in the random component of the error. Despite the signifi-
502 cant efforts in modelling and data assimilation the representation of near-surface tem-
503 perature in the reanalysis is challenging, in particular for daily minimum temperatures.
504 This is likely associated with a large range of limitations in the models representation
505 of clouds, radiation, boundary layer, land surface characteristics, among others. While
506 the random component of the errors were improved in ERA5, likely due to a better syn-
507 optic scale variability and resolution, the still significant systematic biases require fur-
508 ther attention from the modeling perspective.

509 **Acknowledgments**

510 The ERAI reanalysis is available from ECMWF data archive: [https://apps.ecmwf.int/datasets/data/interim-](https://apps.ecmwf.int/datasets/data/interim-full-daily/)
511 [full-daily/](https://apps.ecmwf.int/datasets/data/interim-full-daily/). ERA5 dataset is available from the Copernicus Climate Change Service: <https://climate.copernicus.eu>
512 reanalysis. The observational GHCN dataset was accessed from: [https://www.ncdc.noaa.gov/ghcn-](https://www.ncdc.noaa.gov/ghcn-data-access)
513 [data-access](https://www.ncdc.noaa.gov/ghcn-data-access), and the SNOTEL from: <https://www.wcc.nrcs.usda.gov/snow/>. The sur-
514 face simulations carried out in this study are available from ECMWF data archive (re-
515 quired login at: <https://apps.ecmwf.int/mars-catalogue/?class=rd>) with the research ex-
516 perimental Ids: got2(HTbil), gote(HTdlr), gotf(HTclr), gpob(HTmlr), gpb1 (HTei). This
517 study was funded by the FCT project CONTROL PTDC/CTA-MET/28946/2017. E.

518 Dutra acknowledges the financial support of FCT research grant IF/00817/2015. The
 519 authors acknowledge two anonymous reviewers for their constructive comments and sug-
 520 gestions.

521 References

- 522 Albergel, C., Dutra, E., Munier, S., Calvet, J.-C., Muñoz-Sabater, J., Rosnay, P. d.,
 523 & Balsamo, G. (2018, June). ERA-5 and ERA-Interim driven ISBA land sur-
 524 face model simulations: which one performs better? *Hydrol. Earth Syst. Sci.*,
 525 *22*(6), 3515–3532. doi: 10.5194/hess-22-3515-2018
- 526 Albergel, C., Dutra, E., Muñoz-Sabater, J., Haiden, T., Balsamo, G., Beljaars, A.,
 527 ... Wedi, N. (2015). Soil temperature at ECMWF: An assessment using
 528 ground-based observations. *J. Geophys. Res. D: Atmos.*, *120*, 1361–1373. doi:
 529 10.1002/2014jd022505
- 530 Balsamo, G., Albergel, C., Beljaars, A., Boussetta, S., Brun, E., Cloke, H., ... Vi-
 531 tart, F. (2015). ERA-Interim/Land: a global land surface reanalysis data set.
 532 *Hydrol. Earth Syst. Sci.*, *19*, 389–407. doi: 10.5194/hess-19-389-2015
- 533 Balsamo, G., Viterbo, P., Beljaars, A., Van den Hurk, B., Betts, A. K., & Scipal, K.
 534 (2009). A revised hydrology for the ECMWF model: Verification from field
 535 site to terrestrial water storage and impact in the integrated forecast system.
 536 *J. Hydrometeorol.*, *10*, 623–643 doi: 10.1175/2008JHM1068.1.
- 537 Bechtold, P., Köhler, M., Jung, T., Doblas-Reyes, F., Leutbecher, M., Rodwell,
 538 M. J., ... Balsamo, G. (2008, July). Advances in simulating atmospheric vari-
 539 ability with the ECMWF model: From synoptic to decadal time-scales. *Q.J.R.*
 540 *Meteorol. Soc.*, *134*(634), 1337–1351. doi: 10.1002/qj.289
- 541 Beck, H. E., Pan, M., Roy, T., Weedon, G. P., Pappenberger, F., van Dijk,
 542 A. I. J. M., ... Wood, E. F. (2019, January). Daily evaluation of 26 pre-
 543 cipitation datasets using Stage-IV gauge-radar data for the CONUS. *Hydrol.*
 544 *Earth Syst. Sci.*, *23*(1), 207–224. doi: 10.5194/hess-23-207-2019
- 545 Behnke, R., Vavrus, S., Allstadt, A., Albright, T., Thogmartin, W. E., & Radeloff,
 546 V. C. (2016, July). Evaluation of downscaled, gridded climate data for the con-
 547 terminous united states. *Ecol. Appl.*, *26*(5), 1338–1351. doi: 10.1002/15-1061
- 548 Bernier, N. B., Belair, S., Bilodeau, B., & Tong, L. (2011, October). Near-
 549 Surface and land surface forecast system of the vancouver 2010 winter
 550 olympic and paralympic games. *J. Hydrometeorol.*, *12*, 508–530. doi:
 551 10.1175/2011jhm1250.1
- 552 Cao, B., Gruber, S., & Zhang, T. (2017). REDCAPP (v1.0): Parameterizing val-
 553 ley inversions in air temperature data downscaled from reanalyses. *Geoscientific*
 554 *Model Development*, *10*(8), 2905–2923. doi: 10.5194/gmd-10-2905-2017
- 555 Cosgrove, B. A., Lohmann, D., Mitchell, K. E., Houser, P. R., Wood, E. F., Schaake,
 556 J. C., ... Meng, J. (2003, November). Real-time and retrospective forcing in
 557 the north american land data assimilation system (nldas) project. *J. Geophys.*
 558 *Res.*, *108*(D22), 3. doi: 10.1029/2002JD003118
- 559 Dall’Amico, M., & Hornsteiner, M. (2006, November). A simple method for esti-
 560 mating daily and monthly mean temperatures from daily minima and maxima.
 561 *Int. J. Climatol.*, *26*(13), 1929–1936. doi: 10.1002/joc.1363
- 562 Dee, D. P., Uppala, S. M., Simmons, A. J., Berrisford, P., Poli, P., Kobayashi, S.,
 563 ... Vitart, F. (2011, April). The ERA-Interim reanalysis: configuration and
 564 performance of the data assimilation system. *Q.J.R. Meteorol. Soc.*, *137*(656),
 565 553–597. doi: 10.1002/qj.828
- 566 Dodson, R., & Marks, D. (1997). Daily air temperature interpolated at high spatial
 567 resolution over a large mountainous region. *Clim. Res.*, *8*, 1–20. doi: 10.3354/
 568 cr008001
- 569 Dutra, E., Balsamo, G., Viterbo, P., Miranda, P. M. A., Beljaars, A., Schar, C., &
 570 Elder, K. (2010). An improved snow scheme for the ECMWF land surface

- 571 model: Description and offline validation. *J. Hydrometeorol.*, *11*, 899–916. doi:
572 10.1175/2010JHM1249.1
- 573 Dutra, E., Schär, C., Viterbo, P., & Miranda, P. M. A. (2011). Land-atmosphere
574 coupling associated with snow cover. *Geophys. Res. Lett.*, *38*, L15707. doi: 10
575 .1029/2011gl048435
- 576 Endris, H. S., Omondi, P., Jain, S., Lennard, C., Hewitson, B., Chang’a, L., ...
577 Tazalika, L. (2013, November). Assessment of the performance of CORDEX
578 regional climate models in simulating east african rainfall. *J. Clim.*, *26*(21),
579 8453–8475. doi: 10.1175/JCLI-D-12-00708.1
- 580 Gao, L., Bernhardt, M., & Schulz, K. (2012). Elevation correction of ERA-Interim
581 temperature data in complex terrain. *Hydrol. Earth Syst. Sci.*, *16*, 4661–4673.
582 doi: 10.5194/hess-16-4661-2012
- 583 Gao, L., Bernhardt, M., Schulz, K., & Chen, X. (2017). Elevation correction of
584 ERA-Interim temperature data in the tibetan plateau. *Int. J. Climatol.*, *37*(9),
585 3540–3552. doi: 10.1002/joc.4935
- 586 Gerlitz, L., Conrad, O., Thomas, A., & Böhner, J. (2014). Warming patterns over
587 the tibetan plateau and adjacent lowlands derived from elevation-and bias-
588 corrected ERA-Interim data. *Clim. Res.*, *58*(3), 235–246.
- 589 Hersbach, H., de Rosnay, P., Bell, B., Schepers, D., Simmons, A., Soci, C., ... Zuo,
590 H. (2018). Operational global reanalysis: progress, future directions and syn-
591 ergies with NWP. *ECMWF ERA Report Series*(27), 65pp. Available online:
592 <https://www.ecmwf.int/node/18765>.
- 593 Ioannidou, L., Yu, W., & Bélair, S. (2014). Forecasting of surface winds over eastern
594 canada using the canadian offline land surface modeling system. *J. Appl. Mete-
595 orol. Climatol.*, *53*(7), 1760–1774. doi: 10.1175/JAMC-D-12-0284.1
- 596 Jobst, A. M., Kingston, D. G., Cullen, N. J., & Sirguey, P. (2017). Combining
597 thin-plate spline interpolation with a lapse rate model to produce daily air
598 temperature estimates in a data-sparse alpine catchment. *Int. J. Climatol.*,
599 *37*(1), 214–229. doi: 10.1002/joc.4699
- 600 Liston, G. E., & Elder, K. (2006, April). A meteorological distribution system for
601 High-Resolution terrestrial modeling (MicroMet). *J. Hydrometeorol.*, *7*(2),
602 217–234. doi: 10.1175/JHM486.1
- 603 Maraun, D., Wetterhall, F., Ireson, A. M., Chandler, R. E., Kendon, E. J., Wid-
604 mann, M., ... Thiele-Eich, I. (2010, September). Precipitation downscal-
605 ing under climate change: Recent developments to bridge the gap between
606 dynamical models and the end user. *Rev. Geophys.*, *48*(3), RG3003. doi:
607 10.1029/2009RG000314
- 608 Maselli, F., Pasqui, M., Chirici, G., Chiesi, M., Fibbi, L., Salvati, R., & Corona, P.
609 (2012). Modeling primary production using a 1 km daily meteorological data
610 set. *Clim. Res.*, *54*(3), 271–285.
- 611 Maurer, E. P., Wood, A. W., Adam, J. C., Lettenmaier, D. P., & Nijssen, B. (2002,
612 November). A Long-Term hydrologically based dataset of land surface fluxes
613 and states for the conterminous united states. *J. Clim.*, *15*(22), 3237–3251.
614 doi: 10.1175/1520-0442(2002)015<3237:ALTHBD>2.0.CO;2
- 615 Menne, M. J., Durre, I., Korzeniewski, B., McNeal, S., Thomas, K., Yin, X., ...
616 Houston, T. G. (2012). *Global historical climatology network - daily (GHCN-
617 Daily), version 3*. (Title of the publication associated with this dataset:
618 <https://data.nodc.noaa.gov/cgi-bin/iso?id=gov.noaa.ncdc:C00861>) doi:
619 10.7289/V5D21VHZ
- 620 Menne, M. J., Durre, I., Vose, R. S., Gleason, B. E., & Houston, T. G. (2012,
621 March). An overview of the global historical climatology Network-Daily
622 database. *J. Atmos. Ocean. Technol.*, *29*(7), 897–910. doi: 10.1175/
623 JTECH-D-11-00103.1
- 624 Minder, J. R., Mote, P. W., & Lundquist, J. D. (2010, July). Surface temperature
625 lapse rates over complex terrain: Lessons from the cascade mountains. *J. Geo-*

- 626 *phys. Res.*, 115(D14), F02011. doi: 10.1029/2009JD013493
- 627 Pepin, N. C. (2005). A global comparison of surface and free-air temperatures at
628 high elevations. *J. Geophys. Res.*, 110(D3), 161. doi: 10.1029/2004JD005047
- 629 Shen, Y.-J., Shen, Y., Goetz, J., & Brenning, A. (2016). Spatial-temporal variation
630 of near-surface temperature lapse rates over the tianshan mountains, central
631 asia. *J. Geophys. Res.*, 121(23), 14,006–14,017. doi: 10.1002/2016JD025711
- 632 Sheridan, P., Smith, S., Brown, A., & Vosper, S. (2010). A simple height-based cor-
633 rection for temperature downscaling in complex terrain. *Meteorol. Appl.*, 17,
634 329–339. doi: 10.1002/met.177
- 635 Soares, P. M. M., Cardoso, R. M., Lima, D. C. A., & Miranda, P. M. A. (2017,
636 October). Future precipitation in portugal: high-resolution projections us-
637 ing WRF model and EURO-CORDEX multi-model ensembles. *Clim. Dyn.*,
638 49(7-8), 2503–2530. doi: 10.1007/s00382-016-3455-2
- 639 Soares, P. M. M., Cardoso, R. M., Miranda, P. M. A., de Medeiros, J., Belo-Pereira,
640 M., & Espirito-Santo, F. (2012, November). WRF high resolution dynamical
641 downscaling of ERA-Interim for portugal. *Clim. Dyn.*, 39(9), 2497–2522. doi:
642 10.1007/s00382-012-1315-2
- 643 Stahl, K., Moore, R. D., Floyer, J. A., Asplin, M. G., & McKendry, I. G. (2006,
644 October). Comparison of approaches for spatial interpolation of daily
645 air temperature in a large region with complex topography and highly
646 variable station density. *Agric. For. Meteorol.*, 139(3), 224–236. doi:
647 10.1016/j.agrformet.2006.07.004
- 648 Steinacker, R., Whiteman, C. D., Dorninger, M., Pospichal, B., Eisenbach, S.,
649 Holzer, A. M., ... Baumann, K. (2007, May). A sinkhole field experi-
650 ment in the eastern alps. *Bull. Am. Meteorol. Soc.*, 88(5), 701–716. doi:
651 10.1175/BAMS-88-5-701
- 652 Tobin, C., Rinaldo, A., & Schaefli, B. (2012, June). Snowfall limit forecasts and hy-
653 drological modeling. *J. Hydrometeorol.*, 13(5), 1507–1519. doi: 10.1175/JHM
654 -D-11-0147.1
- 655 Varley, M. J., Beven, K. J., & Oliver, H. R. (1996). MODELLING SOLAR RADI-
656 ATION IN STEEPLY SLOPING TERRAIN. *Int. J. Climatol.*, 16(1), 93–104.
657 doi: 10.1002/(SICI)1097-0088(199601)16:1<93::AID-JOC992>3.0.CO;2-T
- 658 Vosper, S. B., & Brown, A. R. (2008, June). Numerical simulations of sheltering
659 in valleys: The formation of nighttime Cold-Air pools. *Bound.-Layer Meteorol.*,
660 127(3), 429–448. doi: 10.1007/s10546-008-9272-3
- 661 Wang, Y., Wang, L., Li, X., & Chen, D. (2018, March). Temporal and spatial
662 changes in estimated near-surface air temperature lapse rates on tibetan
663 plateau. *Int. J. Climatol.*. doi: 10.1002/joc.5471
- 664 Weiss, A., & Hays, C. J. (2005, January). Calculating daily mean air temperatures
665 by different methods: implications from a non-linear algorithm. *Agric. For.*
666 *Meteorol.*, 128(1), 57–65. doi: 10.1016/j.agrformet.2004.08.008
- 667 Winstral, A., Jonas, T., & Helbig, N. (2017). Statistical downscaling of gridded wind
668 speed data using local topography. *J. Hydrometeorol.*, 18(2), 335–348. doi: 10
669 .1175/JHM-D-16-0054.1

Table 1. Acronyms and description of the elevation correction of ERA5 temperature (top rows) and HTESEL land surface simulations (bottom rows)

Acronym	Description
clr	Elevation correction of ERA5 temperature using a constant ELR of -6.5 K km^{-1}
clr0	Elevation correction of ERA5 temperature using a constant ELR of -4.5 K km^{-1}
mlr	Elevation correction of ERA5 temperature using mean monthly climatological ELR fields derived from ERA5 vertical profiles
dlr	Elevation correction of ERA5 temperature using daily ELR fields derived from ERA5 vertical profiles
HTbil	HTESEL land surface simulation at 9km driven by ERA5 hourly downward fluxes (rainfall, snowfall, longwave and shortwave radiation) and near-surface state (temperature, humidity, wind and pressure). Bilinear interpolation of ERA5 fields from 31 km to 9 km.
HTclr	As HTbil but adjusting ERA5 temperature, humidity and pressure using a constant ELR of -6.5 K km^{-1}
HTmlr	As HTclr but using a mean monthly climatology of ELR fields
HTdlr	As HTclr but using daily ELR fields
HTei	As HTbil but using 3-hourly ERA-Interim downward fluxes and near-surface state. Bilinear interpolation of ERA-Interim fields from 75 km to 9 km.

Table 2. Statistics of the linear regression between elevation differences and temperature differences for the different ELR adjustments and ERA5 original data for the entire period (ALL) and Winter and Summer. In each cell, the top values denotes the slope of the linear regression (K km^{-1}) and the bottom value the correlation coefficient. The bold values highlight corrections with a linear regression slope absolute value below 1 and correlation below -0.4. For each period the 5 columns indicate: constant ELR of -6.5 K km^{-1} (clr), constant ELR of -4.5 K km^{-1} (clr0), mean climatology fields of ELR from ERA5 (mlr), daily ELR fields from ERA5 (dlr) and the original ERA5 data (ERA5).

	ALL					Winter(DJF)					Summer(JJA)				
	ERA5	clr0	clr	mlr	dlr	ERA5	clr0	clr	mlr	dlr	ERA5	clr0	clr	mlr	dlr
dtmax	-6.5	-2.0	0.0	-1.8	-1.4	-4.2	0.3	2.3	-1.3	-0.7	-7.8	-3.3	-1.3	-2.1	-1.8
	-0.9	-0.5	0.0	-0.4	-0.3	-0.6	0.1	0.4	-0.2	-0.4	-0.9	-0.6	-0.3	-0.5	-0.4
dtmean	-4.5	0.0	2.0	0.3	0.6	-2.8	1.7	3.7	0.1	0.6	-5.5	-0.8	1.2	0.4	0.7
	-0.7	0.0	0.4	0.1	0.1	-0.4	0.2	0.5	0.0	0.1	-0.8	-0.2	0.2	0.1	0.2
dtmin	-2.4	2.1	4.1	2.3	2.7	-1.4	3.1	5.1	1.5	2.0	-2.8	1.7	3.7	3.0	3.2
	-0.3	0.3	0.5	0.3	0.3	-0.2	0.3	0.5	0.2	0.2	-0.4	0.2	0.4	0.4	0.4

Figure 1. ERA5 orography differences in respect to the stations elevation of GHCN (a), SNOTEL snow depth (b) and SNOTEL soil temperature (c)

Figure 2. Comparison of ELR (Γ) derived from ERA5 vertical profiles and estimated from the stations observation over the WUS domain. ERA5 versus dtmean station ELR for each grid point considering the full period (a: June 2009-May 2014) summer (b) and winter (c). d) Mean annual cycle of ELR averaged over WUS domain given by ERA5 (black line) and station data computed with dtmax (dashed red), dtmean (solid red) and dtmin (dotted red). Spatial distribution of ELR for the full period using dtmean from the station data (e) and ERA5 (f). In panels a-c the slope of the linear fit (S and dashed line) and correlation coefficient (R) are displayed in the legend.

Figure 3. Temperature differences between ERA5 and observations as a function of the station elevation differences (ERA5-station) for dtmax (a), dtmean (b) and dtmin (c) considering the full period. The scatter plots display ERA5 (black), ERA5 with a constant Γ correction of -6.5 K km^{-1} (clr, grey), ERA5 with a constant Γ correction of -4.5 K km^{-1} (clrO, light grey), ERA5 with a climatological Γ correction (mlr, red) and ERA5 with a daily Γ correction (blue). In each panel the legend displays the slope (S) of the linear best-fit and correlation coefficient (R).

Figure 4. Median bias (a-c), normalized STDE (d-f) and normalized MAE (g-i) of ERA5 and the different ELR corrections of dtmax (top panels), dtmean (middle panels) and dtmin (bottom panels). The bars represent the median of the station scores computed for different periods (horizontal axes: all period:YEAR, DJF, and JJA) and the error bars denote the 95% confidence intervals from 1000 samples bootstrapping. The STDE and MAE were normalized by those of ERA5, shown above the bars. The statistics were computed using all 2941 stations with a mean elevation difference between ERA5 orography and stations of 28 meters.

Figure 5. Median bias of ERA5 and the different ELR corrections of dtmax (top panels), dtmean (middle panels) and dtmin (bottom panels), considering stations above ERA5 orography a-c (elevation differences $>300 \text{ m}$, 385 stations with a mean elevation differences of -475 m) and below ERA5 orography d-f (elevation differences $<300 \text{ m}$, 494 stations with a mean elevation difference of 450 m). The bars represent the median of the station scores computed for different periods (horizontal axes: all period:YEAR, DJF, and JJA) and the error bars denote the 95% confidence intervals from 1000 samples bootstrapping. The STDE and MAE were normalized by those of ERA5, shown above the bars.

Figure 6. Surface only simulations evaluation of soil temperature at 5 cm deep: mean bias (a), normalized mae (b), normalized sdte (c) and correlation coefficient differences in respect to ERAI (d). The bars represent the median of the stations scores computed for different periods (horizontal axes: all period: YEAR, DJF and JJA) and the error bars denote the 95% confidence interval from 1000 samples bootstrapping. The mae and stde were normalized by those of ERAI, shown above of the bars. In the bias, the light blue bars (first from the left) denote ERAI. The statistics were computed using 260 stations with a mean elevation difference between ERA5 orography and the stations of -460 meters .

Figure 7. As Figure 6 but for snow depth. The horizontal axis show the scores for the full period (YEAR), only Winter (DJF) and only Spring (MAM). The statistics were computed using 313 stations with a mean elevation difference between ERA5 orography and the stations of -413 meters.

Figure 8. Observations temperature errors estimate dependence on resolution. (a) The number of areas used for each search radius (left axis, black) and mean number of stations in each (right axis, grey), considering all stations (squares) in a neighborhood radius (horizontal axis) or only stations in the neighborhood with a similar altitude (within 100m, in triangles). Estimate of Mean absolute error (b) and standard deviation of the error (c) of the mean compared with the neighborhood stations for different search radius. In panels (b) and (c) the color indicate dtmean (black), dtmax (red) and dtmin (blue) while the solid lines indicate that all stations in the neighborhood radius are used while dashed lines indicate that only stations with a similar altitude were considered. Panels (b) and (c) also show the errors estimates of ERAI (at 75km), and ERA5 (at 31 km) as stars connected by a dotted line. The ERAI and ERA5 estimates were computed only for stations with an altitude difference lower than 100m to both ERAI and ERA5 orography (588 stations)

Figure 1.

Accepted Article

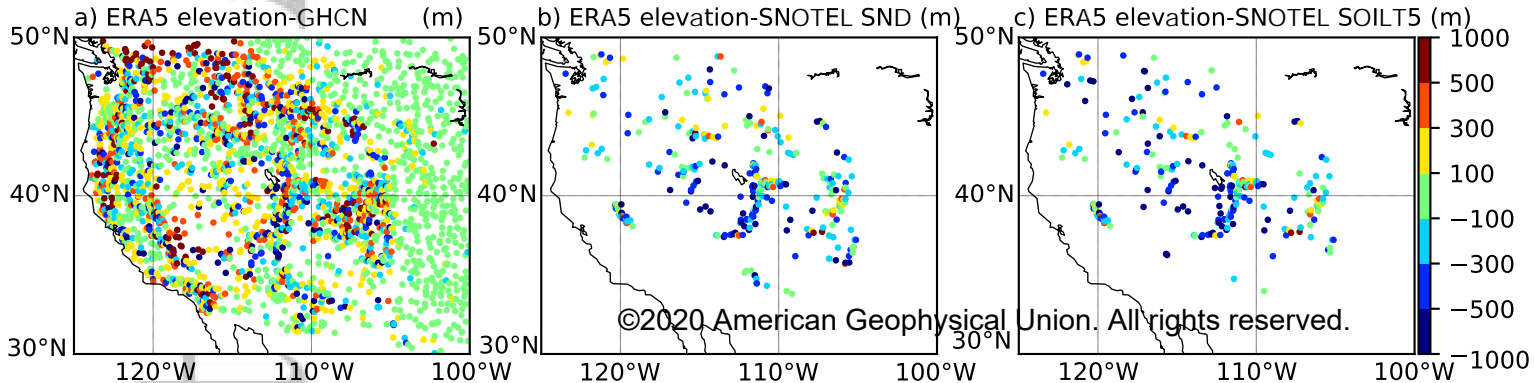


Figure 2.

Accepted Article

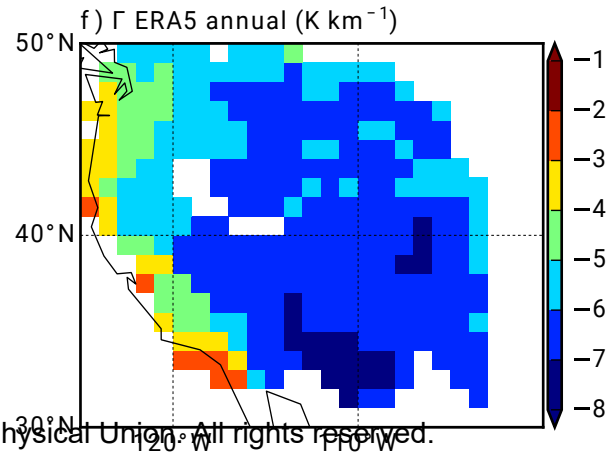
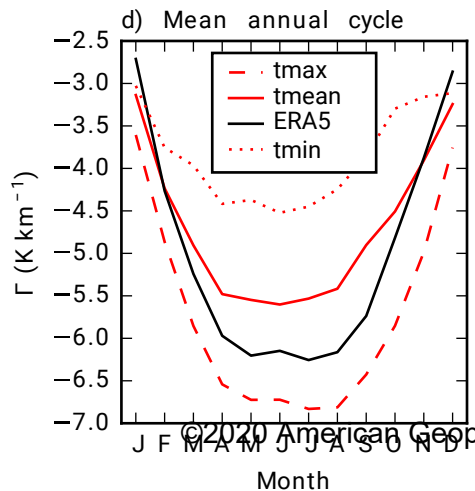
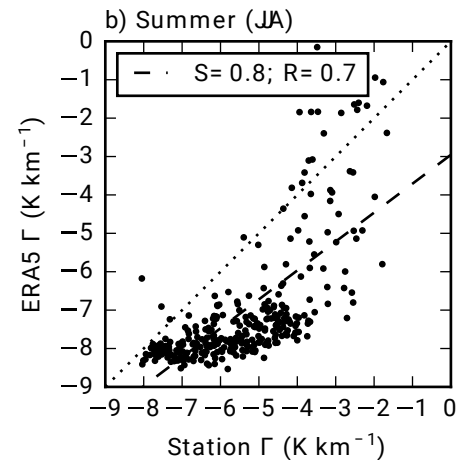
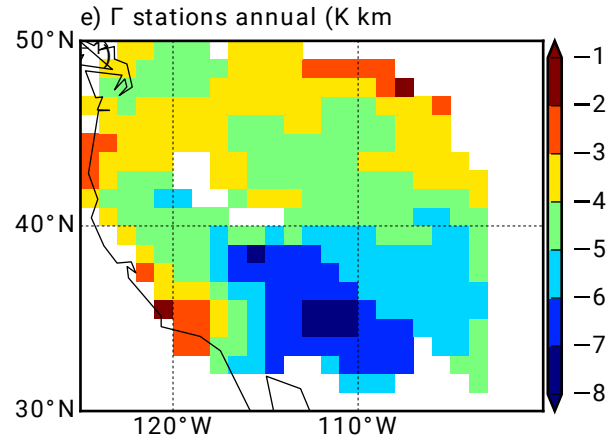
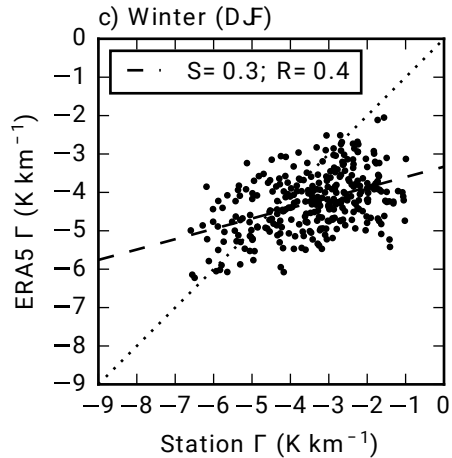
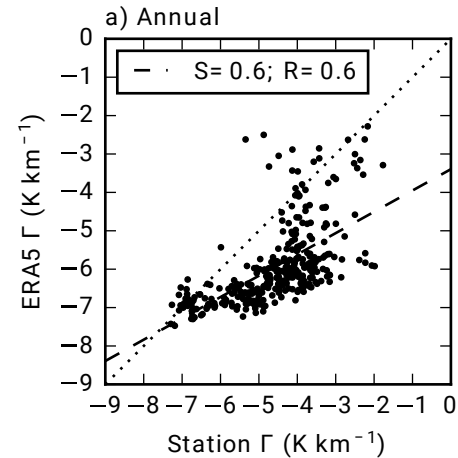
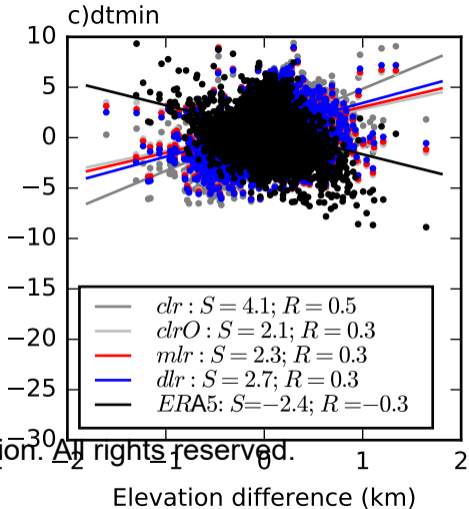
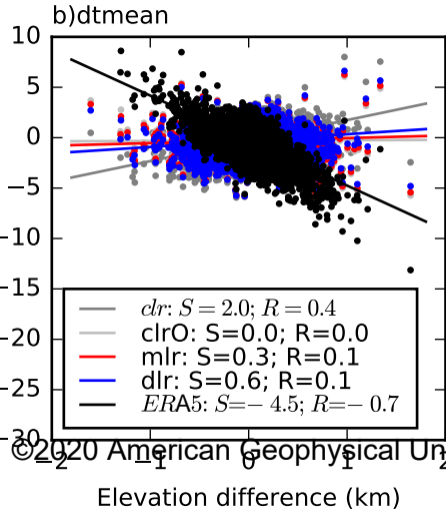
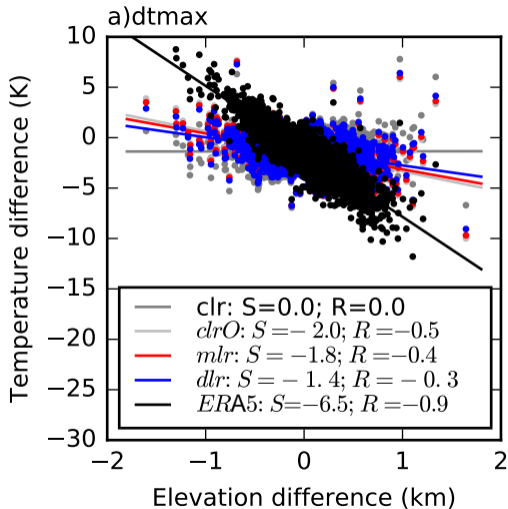


Figure 3.

Accepted Article



©2020 American Geophysical Union. All rights reserved.

Figure 4.

Accepted Article

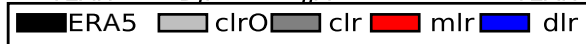
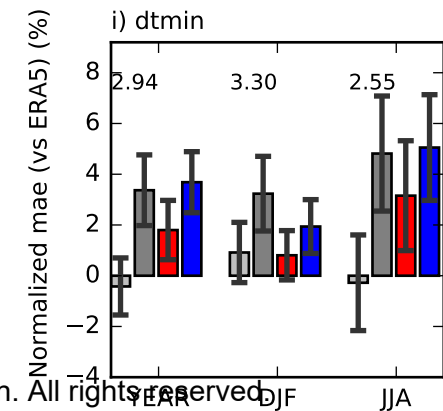
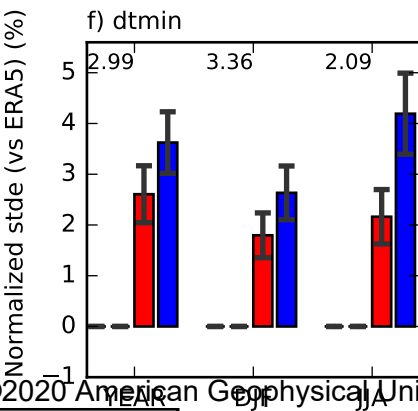
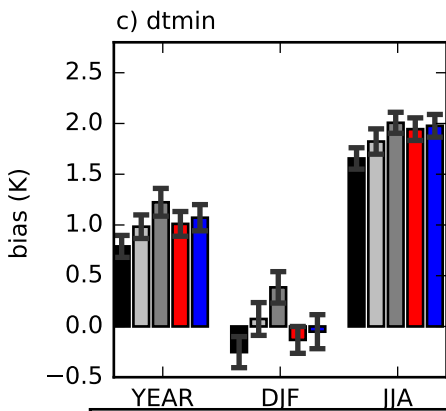
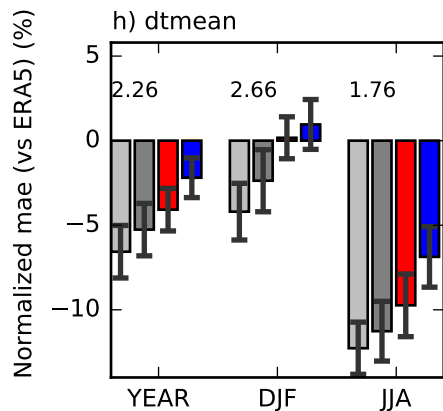
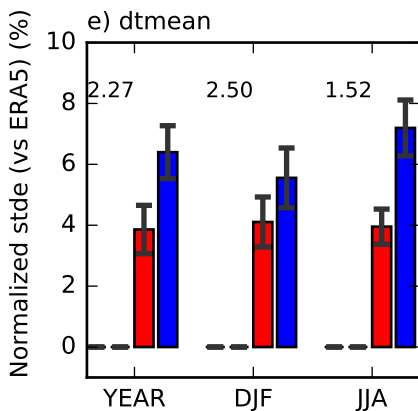
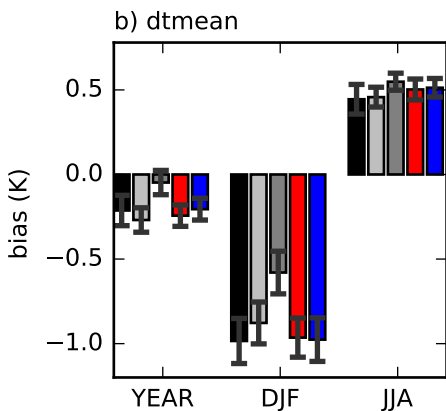
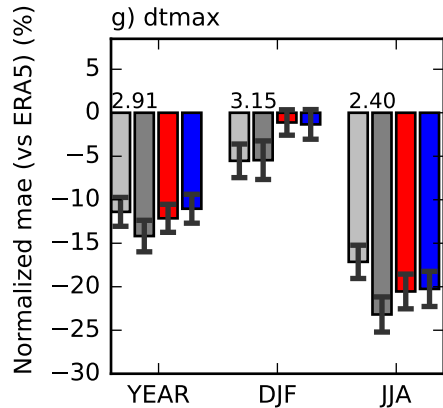
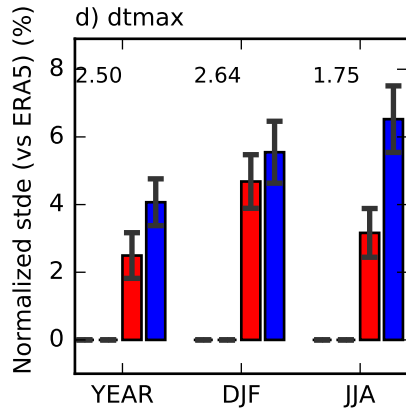
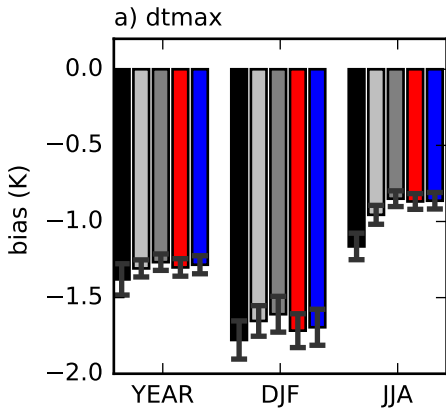
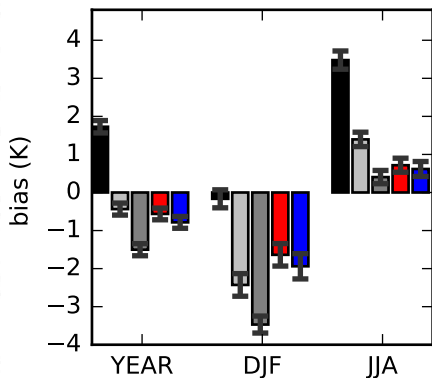


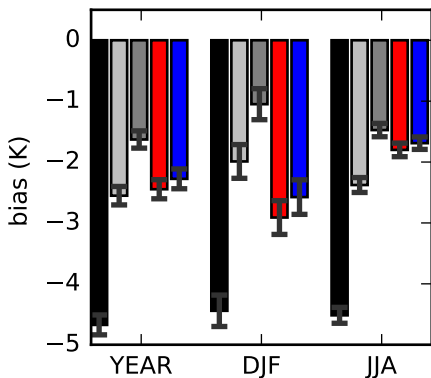
Figure 5.

Accepted Article

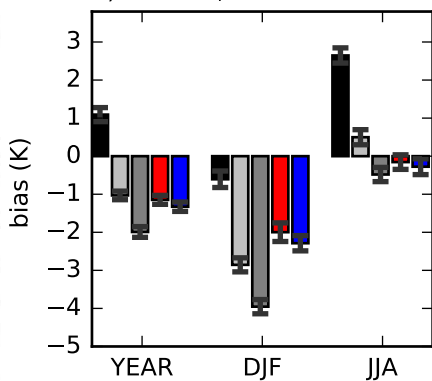
a) dtmax, above



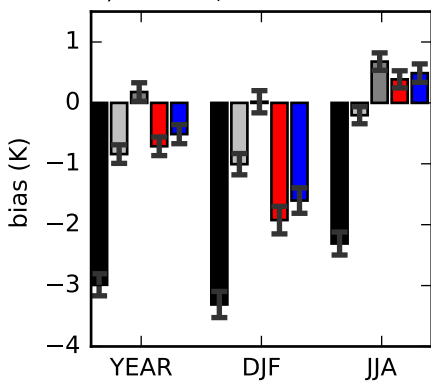
d) dtmax, below



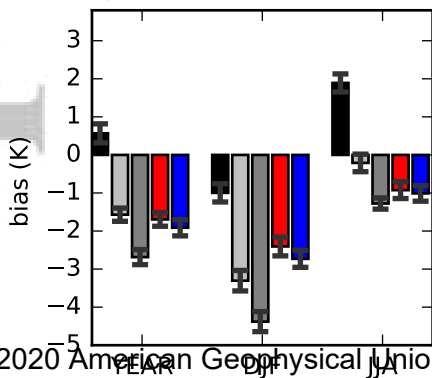
b) dtmean, above



e) dtmean, below



c) dtmin, above



f) dtmin, below

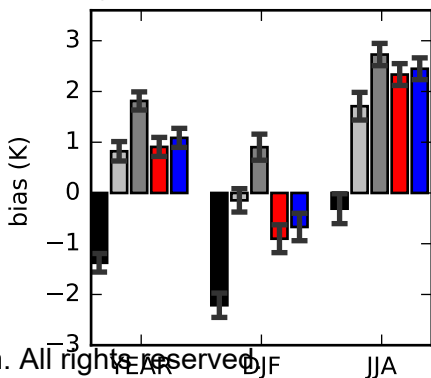
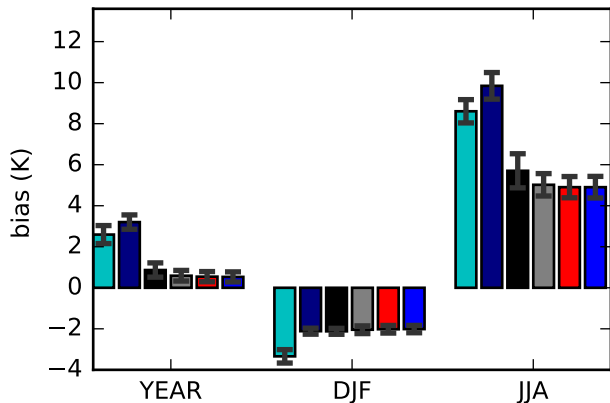


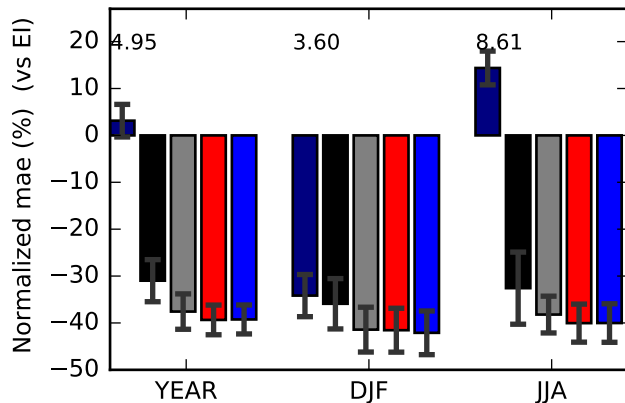
Figure 6.

Accepted Article

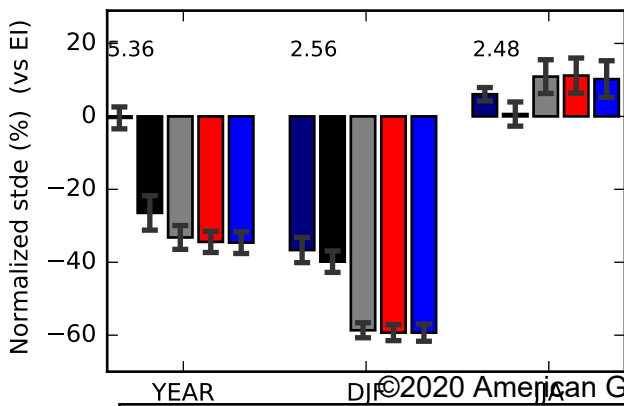
a) bias: SOILT5



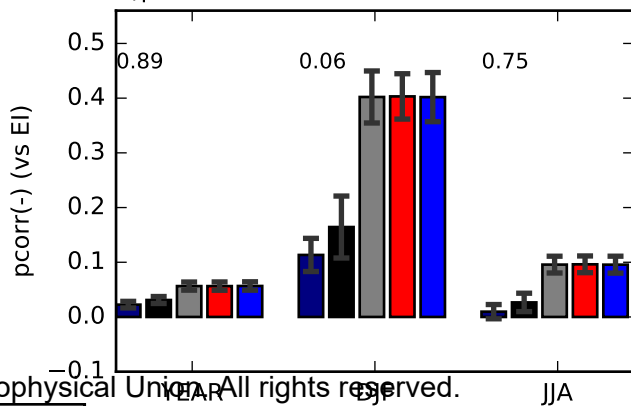
c) Nmae:SOILT5



b) Nstde:SOILT5



d) pcorr: SOILT5



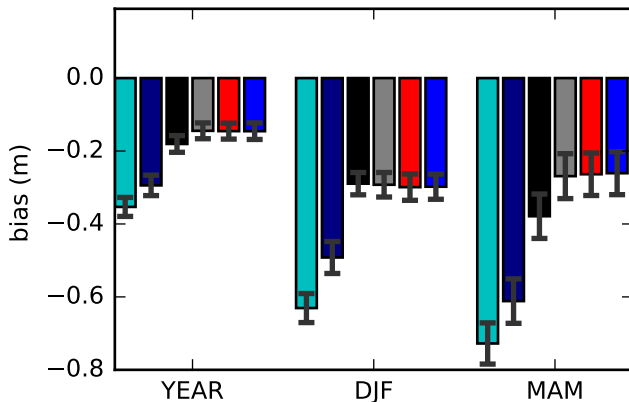
©2020 American Geophysical Union. All rights reserved.



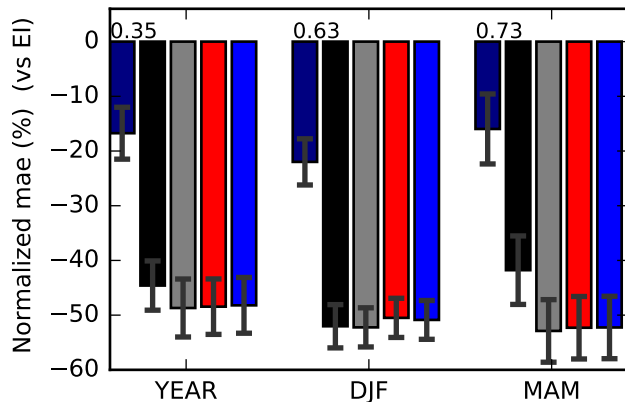
Figure 7.

Accepted Article

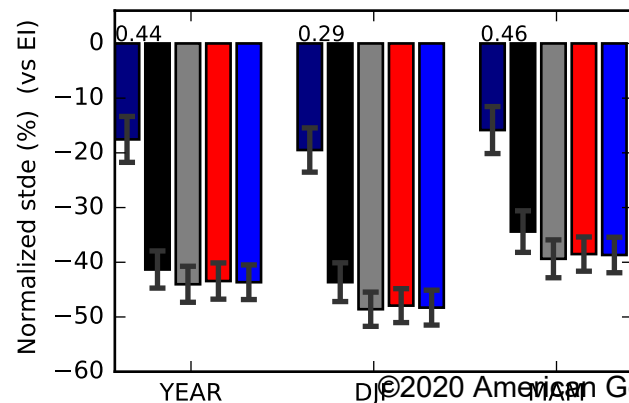
a) bias: SND



c) Nmae: SND



b) Nstde: SND



d) pcorr: SND

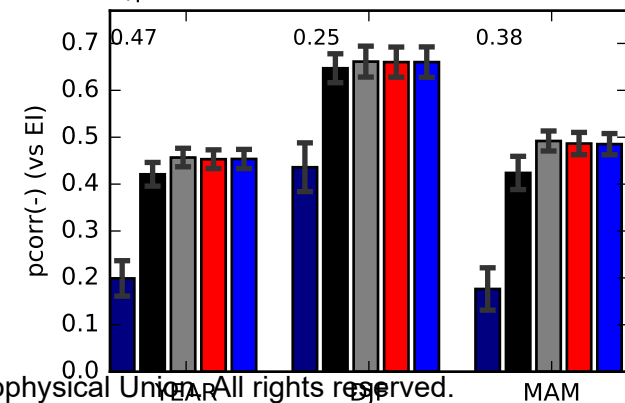


Figure 8.

Accepted Article

